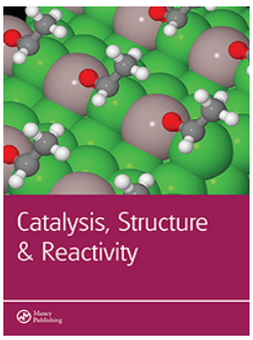

Catalysis, Structure & Reactivity

ISSN: 2055-074X (Print) 2055-0758 (Online) Journal homepage: http://www.tandfonline.com/loi/ycsr20

Photocatalytic hydrogen production by reforming of methanol using Au/TiO_2, Ag/TiO_2 and $Au-Ag/TiO_2$ catalysts

Julia Kennedy, Wilm Jones, David J. Morgan, Michael Bowker, Li Lu, Christopher J. Kiely, Peter P. Wells & Nikolaos Dimitratos

To cite this article: Julia Kennedy, Wilm Jones, David J. Morgan, Michael Bowker, Li Lu, Christopher J. Kiely, Peter P. Wells & Nikolaos Dimitratos (2015) Photocatalytic hydrogen production by reforming of methanol using Au/TiO_2, Ag/TiO_2 and $Au-Ag/TiO_2$ catalysts, Catalysis, Structure & Reactivity, 1:1, 35-43, DOI: 10.1179/2055075814Y.0000000006

To link to this article: http://dx.doi.org/10.1179/2055075814Y.0000000006

Catalysis, Structure & Reactivity

Original Research Paper

Photocatalytic hydrogen production by reforming of methanol using Au/TiO_2, Ag/TiO_2 and Au-Ag/TiO_2 catalysts

Julia Kennedy[1], Wilm Jones[2], David J. Morgan[1], Michael Bowker*[1,2], Li Lu[4], Christopher J. Kiely[4], Peter P. Wells[2,3] and Nikolaos Dimitratos*[1,2]

[1]Cardiff Catalysis Institute, School of Chemistry, Cardiff University, Main Building, Park Place, Cardiff CF10 3AT, UK
[2]UK Catalysis Hub, Research Complex at Harwell (RCaH), Rutherford Appleton Laboratory, Harwell, Oxon OX11 0FA, UK
[3]Department of Chemistry, UCL, 20 Gordon St., London WC1H 0AJ, UK
[4]Department of Materials Science and Engineering, Lehigh University, 5 East Packer Avenue, Bethlehem, PA 18015, USA

Abstract We have investigated polyvinylalcohol stabilized Au and Ag based nanoparticles supported on titania prepared via sol immobilisation for the anaerobic, ambient temperature reforming of methanol with water for the photocatalytic production of hydrogen. The catalytic activity of the Au/TiO_2 catalysts was strongly affected by the metal loading and calcination temperature. Here, we report the preparation and use of supported Au–Ag nanoparticles, based on either the co-reduction or the consecutive reduction of the two metals. Au–Ag supported catalysts were more active than monometallic Au and Ag catalysts and the preparation methodology had a pronounced effect in terms of catalytic activity of the Au–Ag catalysts. In fact, using a consecutive reduction where Au was firstly reduced followed by reduction of Ag gave materials which exhibited the highest catalytic performance.

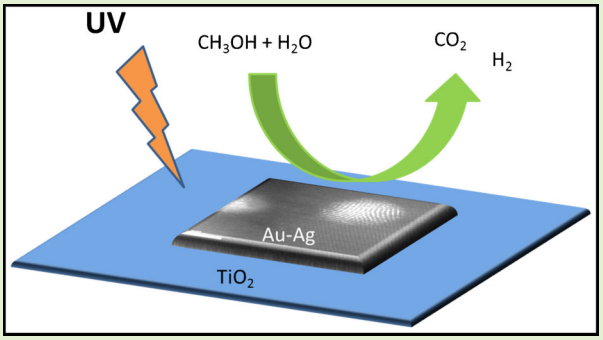

Keywords Supported gold and silver nanoparticles, Photocatalytic hydrogen production, Sol immobilization

Cite this article J. Kennedy, W. Jones, D. J. Morgan, M. Bowker, L. Lu, C. J. Kiely, P. P. Wells and N. Dimitratos: *Catal. Struct. React.*, 2015, 1, 35-43

Introduction

We are in a period of great turbulence in relation to the energy supply needs of the human population of the globe. Not only are easily accessible fossil fuel supplies dwindling, but we are more aware than ever of the deleterious effects of such combustion processes. We have seen a massive increase in CO_2 loading in the atmosphere due to the burning of fossil fuels, up from 280 ppm in recent geological history to ~380 ppm now, a 36% increase in a relatively short time. Whatever the bias is regarding the effects on global warming, this strategy – that is, to burn-up, in a couple of hundred years all of the carbon that was removed from the atmosphere over ~100 million years during the Carboniferous period – cannot be a sensible strategy. During that period, atmospheric CO_2 decreased from ~5000 to ~280 ppm, a huge decrease, and oxygen levels in the atmosphere increased. Fracking shale to produce combustible gas is a strategy of high risk that will only push up the atmospheric CO_2 load even further.

Hence there is a critical need to find and develop alternative fuel sources, which are as sustainable and as non-polluting as possible and there are none better for this purpose than solar production of hydrogen. If we can use solar energy to split water, then we have a virtuous cycle of H_2+O_2 production, followed by combustion back to water. However, as we outlined in a recent review[1] there are great difficulties with direct water splitting, most notably the high endothermicity (+240 kJ mol^{-1}) of the reaction and the ease of the back reaction. Hence, alternative strategies include the use of biofuels use as sacrificial agents to both split water and provide for extra H_2 production. Although CO_2

*Corresponding authors, email sacnd1@cardiff.ac.uk; bowkerm@cf.ac.uk

Received 28 August 2014; accepted 12 November 2014
DOI 10.1179/2055075814Y.0000000006

is produced in such a process, that CO_2 is not from fossil fuels and can represent a recycling of CO_2 from the atmosphere, while reducing net emissions into the atmosphere (by use of the H_2 so produced for fuel cells or combustion).

The main photocatalytic substrates are generally semiconductors which interact with the incident radiation by the creation of electron–hole pairs which are subsequently separated to be utilized in reduction and oxidation steps, with the most promising materials to date being based on titania catalysts. However, a drawback of these titania catalysts is their poor photocatalytic efficiency due to unwanted recombination of the electron–hole pairs.[2,3] One of the main approaches to improve the efficiency of such materials is the addition of metal nanoparticles onto the titania surface which can trap electrons and lessen the recombination of electron–hole pairs.[4–6] It has been shown that gold based nanoparticles supported on metal oxides and particularly the combination of gold and palladium/platinum exhibit high conversion for the selective transformation of organic compounds, such as the oxidation of carbon monoxide, alkanes, alcohols and polyols.[7–11] Silver based nanoparticles have also received extensive consideration due to their use in a range of potential applications, such as microelectronics, sensing and catalysis.[12–17] This paper continues our work on photocatalytic titania[12–21] but reports on the incorporation of nanoparticles (supported Au and Au–Ag nanoparticles) produced by the sol immobilization method. With this methodology, the synthesis of gold based nanoparticles with particle diameters below 10 nm with controlled morphology (random alloy or core–shell structures) is achievable.[22–27] Furthermore, the synthesis of supported Au–Ag nanoparticles was achieved by developing experimental protocols based on the simultaneous reduction or successive reduction of metallic precursors.

Experimental

Catalyst preparation

Sol immobilization method

Au, Ag and Au–Ag nanoparticles supported on TiO_2 (P25-Degussa) were prepared using a sol immobilization method. Au/TiO_2 and Ag/TiO_2 catalysts were synthesized as follows. An aqueous solution of $AgNO_3$ or $HAuCl_4.3H_2O$ (Johnson Matthey) of the desired concentration (1.3×10^{-4}M) was prepared. To this solution polyvinylalcohol (PVA) (1 wt-% solution, Aldrich, weight average molecular weight M_W= 9000–10 000 g mol^{-1}, 80% hydrolysed) was added (PVA/M (M=Au or Ag) (wt/wt)=0.65). Subsequently, 0.1M of freshly prepared solution of $NaBH_4$ (>96%, Aldrich, $NaBH_4$/M (M=Au or Ag) (mol/mol)=5) was then added to form a sol. After 30 min of sol generation, the colloid was immobilized by adding TiO_2 (acidified to pH 1 by sulfuric acid) under vigorous stirring conditions. The amount of support material required was calculated so as to have a total final metal loading varying in the range from 0.1 to 5 wt-%. After 2 h the slurry was filtered, the catalyst was washed thoroughly with distilled water and then dried at 120°C overnight. The sets of dried catalysts were also calcined in the 200–400°C temperature range in static air using a muffle oven (ramp rate 5°C min^{-1}) for 3 h.

Three methods were used for the preparation of sol immobilized Au–Ag catalysts which differ in the sequence of metal addition and reduction. For the preparation of (Au–Ag)/TiO_2 materials an aqueous solution of $AgNO_3$ and $HAuCl_4.3H_2O$ (Johnson Matthey) of the desired concentration were prepared. Polyvinylalcohol (1 wt-% aqueous solution, Aldrich, MW=9000–10 000 g mol^{-1}, 80% hydrolysed) and an aqueous solution of $NaBH_4$ (0.1M) were also prepared.

Method A: Au+Ag sol

To an aqueous $AgNO_3$ and $HAuCl_4$ solution of the desired concentration (1.3×10^{-4}M), the required amount of a PVA solution (1 wt-%) was added (PVA/(Au+Ag) (wt/wt)=1.2); a freshly prepared solution of $NaBH_4$ (0.1M, $NaBH_4$/(Au+Ag) (mol/mol)=5) was then added to form a sol.

Method B: Ag{Au} sol

To an aqueous $HAuCl_4$ solution of the desired concentration the required amount of a PVA solution (1 wt-%) was added (PVA/(Au+Ag) (wt/wt)=1.2, corresponding to the total final amount of metal present); a freshly prepared solution of $NaBH_4$ (0.1M, $NaBH_4$/Au (mol/mol)=5) was then added to form a sol. The solution was stirred for 30 min. Then, the required amount of the stock aqueous $AgNO_3$ solution was added, followed by the desired amount of $NaBH_4$ ($NaBH_4$/Ag (mol/mol)=5), obtaining a sol. The solution was stirred for a further 30 min.

Method C: Au{Ag} sol

To an aqueous $AgNO_3$ solution of the desired concentration the required amount of a PVA solution (1 wt-%) was added (PVA/(Au+Ag) (wt/wt)=1.2, corresponding to the total final amount of metal present); a 0.1M freshly prepared solution of $NaBH_4$ ($NaBH_4$/Ag (mol/mol)=5) was then added to form a sol. The solution was stirred for 30 min. Then, the desired amount of the stock $HAuCl_4$ aqueous solution was added, followed by the desired amount of $NaBH_4$ ($NaBH_4$/Au (mol/mol)=5), obtaining a sol. The solution was stirred for further 30 min.

Supported catalysts

After 30 min of sol generation, the colloid was immobilized by adding TiO_2 (acidified at pH 1 by sulfuric acid) under vigorous stirring conditions. The amount of TiO_2 support material required was calculated so as to have a total final metal loading of 1 wt-%. The metal ratio for the 1 wt-%Au+Ag/TiO_2 catalyst was 1:1 molar. After 2 h the slurry was filtered, the catalyst was washed thoroughly with distilled water (neutral mother liquors) to remove all the dissolvable species, (such as Na^+ or Cl^-) and the powder was collected and dried at 120°C overnight.

Nanoparticle characterization

UV–visible spectroscopy of the colloidal sols was used to monitor the intensity and position of the plasmon resonance band of Au, Ag and Au–Ag colloids. Samples for examination by transmission electron microscopy (TEM) were prepared by dispersing the dry catalyst powder in high purity ethanol, followed by sonication. A drop of this suspension was then evaporated onto a holey carbon film supported by a 300 mesh copper TEM grid. The instrument used for this analysis was a JEOL 2100 LaB_6 TEM operating at 200 kV. STEM high

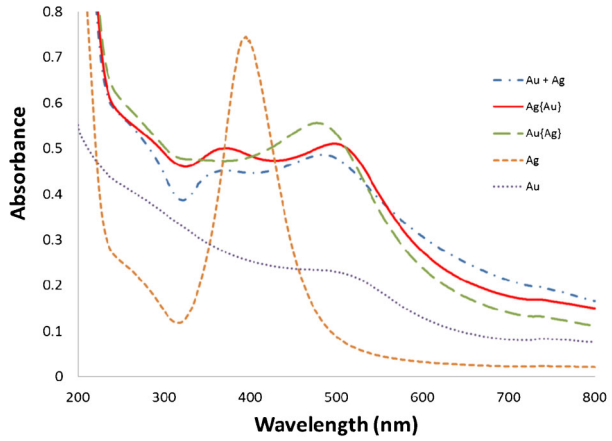

Figure 1 UV–vis spectra obtained from various Au. Ag, Au–Ag colloidal solutions

angle annular dark field (HAADF) images of the Au–Ag particles were obtained using an aberration corrected ARM 200 FS(S)TEM operating at 200 kV.

X-ray photoelectron spectra were recorded on a Kratos Axis Ultra DLD spectrometer employing a monochromatic Al K_α X-ray source (75–150 W) and analyzer pass energies of 160 eV (for survey scans) or 40 eV (for detailed scans). Samples were mounted using double sided adhesive tape and binding energies referenced to the C(1s) binding energy of adventitious carbon contamination which was taken to be 284.7 eV.

Catalytic reactions

Photocatalytic reactions were conducted in the liquid phase in a Pyrex flask under an argon atmosphere. The catalysts were sieved before catalytic testing through a stainless steel mesh (to<53 μm) and were placed in 100 mL of deionized water containing 110 μL (2718 μmoL) of methanol (Fisher Scientific 99.99%) in a glass reactor. The mixture was purged for 30 min with argon to remove dissolved gases and the reactor was finally sealed under argon before switching on the light source (400 W Xe arc, Oriel Model 66084) in the UV range. The product analysis for H_2 was carried out by using a Varian 3300 gas chromatograph with a thermal conductivity detector and a 2 m MS 13X column. The conversion levels for methanol were in the 1–12% range for the majority of the dried catalysts studied and the 1–33% range for the majority of the calcined catalysts.

Results and discussion

Preparation and characterization of Au, Ag and Au–Ag nanoparticles

A range of Au, Ag and Au–Ag colloidal sols were synthesized and immobilized on TiO_2. For the monometallic catalysts UV analysis showed the appearance of the plasmon resonance peaks centered at 514 nm for colloidal Au and 397 nm for colloidal Ag (Fig. 1). These resonance peak positions are characteristic of gold and silver nanoparticles in the sub-10 nm particle size regime.[28,29] In the case of the Au{Ag} sol we observed the disappearance of the Ag peak and a blue shift of the Au peak, and the appearance of a new peak at 479 nm, which is indicative of either a Au–Ag alloy or of a core–shell structure with a thick Au shell, since only the plasmon resonance peak of the metal constituting the shell should be observed.[30,31] For the Ag{Au} sols two peaks were observed at 499 and 373 nm with similar intensity, which suggests the presence of a thin shell of Ag (since the plasmon peak of the core metal could be observed[30]) and the presence of either an Au–Ag alloy or possibly of Ag nanoparticles. Finally, in the case of the Au + Ag sol, the shift and the presence of two peaks at 484 and 372 nm was observed suggesting the simultaneous presence of Au–Ag alloy and Ag nanoparticles.[32] Mallin and Murphy[33] demonstrated that by using sodium citrate as the capping agent and by varying the molar ratio of Au/Ag, alloy nanoparticles could be formed. The absorbance peak was dependent on the Au/Ag metal ratio and was found to be in the 430–505 nm range. Jiang and co-workers[34] used HAADF–STEM analysis to show the formation of Au_{core}–Ag_{shell} nanoparticles immobilized on a metal organic framework.

Representative bright field TEM micrographs of our materials were acquired in order to characterize the particle size distributions of the colloidal metal nanoparticles after immobilization and drying or calcination on the TiO_2 support. The particle size data for all the catalysts studied are summarized in Tables 1 and 2. In all cases the colloidal particles are homogeneously dispersed over the TiO_2. The particle size distributions for the monometallic Au/TiO_2 dried catalysts with Au loadings ranging from 0.25 to 5 wt-% are shown in Figs. S1 and S2 in the Supplementary Material. The Au mean particle sizes were found to be in the 2.9 to 4.4 nm range respectively and the vast majority of the particles were smaller than 10 nm. For the calcined Au/TiO_2 materials, the mean particle size increased from 4 to 6–7 nm (Figs. S3 and S4, Supplementary Material), implying that the Au particles on TiO_2 exhibited a small degree of sintering at 400°C and we have previously reported that this coincides with the development of a strong metal support interaction[35] as shown in Fig. 2. It is evident that upon increasing the calcination temperature the shape of gold particles changed from spherical to hemispherical and the particles form an extended flat interface structure with the TiO_2 support, thereby increasing the number of support/particle periphery sites (Fig. 2*b*). For the 1 wt-% supported Au–Ag catalysts, the particle size distribution data (Fig. 3) showed that the mean

Table 1 Mean particle sizes as determined from TEM measurements of various immobilized supported Au catalysts investigated in our photocatalytic experiments

wt-%Au/TiO_2 (dried at 120°C)	0.1	0.25	0.4	0.5	0.7	1	2	5
Mean particle size and standard deviation values	n.d.	2.9±0.8	2.9±0.8	3.3±1.0	3.1±0.9	2.9±0.7	3.5±1.2	4.4±1.7
wt-%Au/TiO_2 (calcined at 400°C)	0.1	0.25	0.4	0.5	0.7	1	2	5
Mean particle size and standard deviation values	n.d.	4.4±1.1	4.2±0.9	4.9±1.4	4.6±1.2	5.5±1.5	4.6±1.4	6.7±1.9

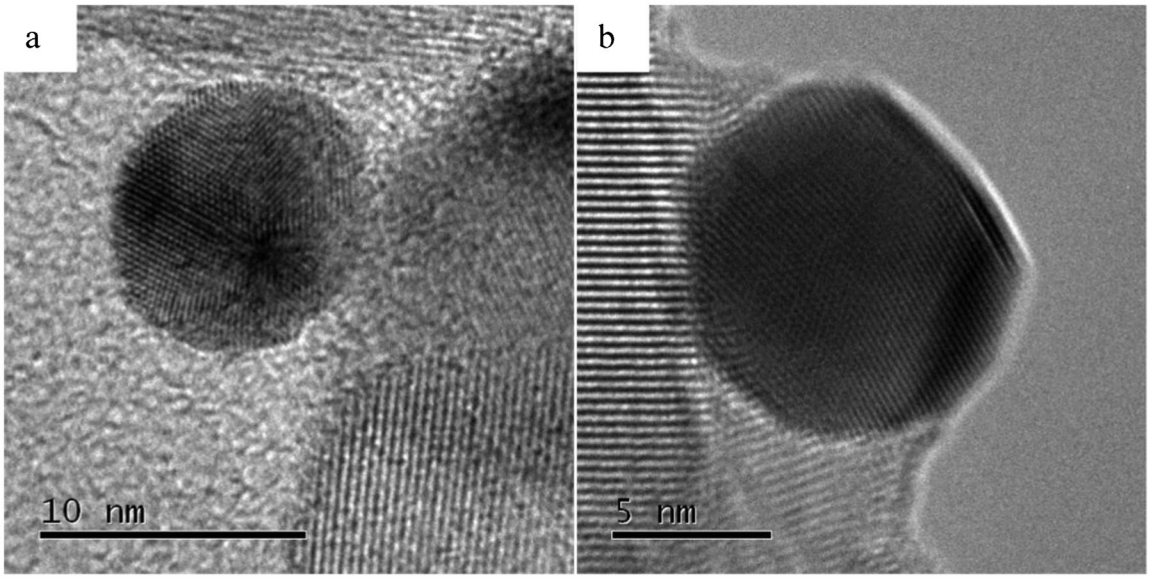

Figure 2 Representative HREM micrographs of Au particles on *a* dried and *b* calcined 1 wt-%Au/TiO_2 catalysts

particle sizes were around 4 nm. Comparison with the monometallic 1 wt-%Ag supported catalysts (Table 2) showed that a significant decrease in the mean particle size from 8.7 to 4 nm was achieved by mixing Ag with Au either by co-reduction or consecutive reduction. This is direct evidence for the formation of bimetallic particles. Furthermore, no bimodal distributions were found, which should be the case if mixtures of single metal (Au and Ag) particles were present. The Au–Ag catalysts were further characterized by aberration corrected scanning transmission electron microscopy in an attempt to glean information about the elemental distribution within individual nanoparticles. Figure 4 shows representative low magnification STEM–HAADF images of the synthesized Au–Ag catalysts along with some higher magnification BF– and HAADF–STEM pairs of images from individual Au–Ag particles. In the HAADF imaging technique if a distinct core–shell structure is present, it is sometimes visible through mass contrast since Au ($z=79$) and Ag ($z=47$) have a considerable difference in atomic number. In the 1 wt-%Au + Ag/TiO_2 sample prepared by co-reduction (Fig. 4*a–c*) there is only a very slight HAADF contrast decrease at the periphery of these particles due to the expected projected thickness variation (Fig. 4*c*), which suggests that the majority of the particles are homogeneous random alloys. In the 1 wt-%Ag{Au}/TiO_2 catalyst (Fig. 4*g–i*) some of the particles showed a more distinct decrease in HAADF intensity at the particle periphery, (e.g. see Fig 4*i*), implying the probable existence of a Au-rich core and Ag-rich shell. For the 1 wt-%Au{Ag}/TiO_2 catalyst (see Fig. 4*d–f*) some of the particles showed a very slight decrease in HAADF intensity at the particle center (Fig. 4*f*), which could be interpreted as a Ag-rich core and Au-rich shell morphology in agreement with the UV data.

Table 3 shows XPS data for all of the monometallic Au/TiO_2, Ag/TiO_2 and Au–Ag/TiO_2 catalyst variants and Fig. 5 shows the Ag(3d) and the Au(4f) spectra of the Ag{Au}/TiO_2 catalyst as a representative example. For the samples studied the XPS data confirmed the presence of metallic gold with an Au $4f_{7/2}$ peak observed at a binding energy of 83.2–83.6 eV, whereas for the silver the data confirmed the presence of silver in a positive oxidation state (Ag^+) in agreement with previous reports.[32] The absence of metallic Ag is mainly due to oxidation during the drying process which involves exposure to air. The surface Au/Ag atomic ratios suggested (Table 3) that for the Au + Ag/TiO_2 and Au{Ag}/TiO_2 catalysts the surface of the bimetallic nanoparticles are enriched with Au, whereas for the Ag{Au}/TiO_2 catalyst variant a significant drop in the Au/Ag atomic ratio was observed, implying Ag surface enrichment on that sample in agreement with our STEM studies. Taking into account the standard reduction potentials of Au and Ag in solution at room temperature [E° Au^{3+}/Au=0.93 V(SHE), E° Ag^+/Ag=0.8 V(SHE)] we expect that the Au^{3+} and Ag^+ ions should be reduced quickly by the addition of excess amount of $NaBH_4$. Furthermore, since the reduction potential of Au is higher (i.e. more positive) than that of Ag, it is plausible that Au^{3+} would be reduced more easily during the nucleation process.[34] On the other hand, for the Ag species only a one-electron reduction is required, which is kinetically much easier than a multi-electron reduction, which slows down the reduction rate. An additional parameter to consider is the surface energy of Au (1.5 J m^{-2}) and Ag (1.25 J m^{-2}). In general, for bimetallic systems the component with the lower surface energy has a tendency to accumulate on surface. However, this statement does not necessarily apply for reactions occurring in solution, where the surface

Table 2 Mean particle sizes as determined from TEM measurements of various Au, Ag and Au–Ag nanoparticles immobilized on TiO_2 investigated in our photocatalytic experiments

1 wt-%metal/TiO_2 (dried at 120°C)	Au only	Au + Ag	Ag{Au}	Au{Ag}	Ag only
Mean particle size and standard deviation values	2.9 ± 0.7	3.9 ± 1.3	3.9 ± 1.5	4.0 ± 1.6	8.7 ± 4.1

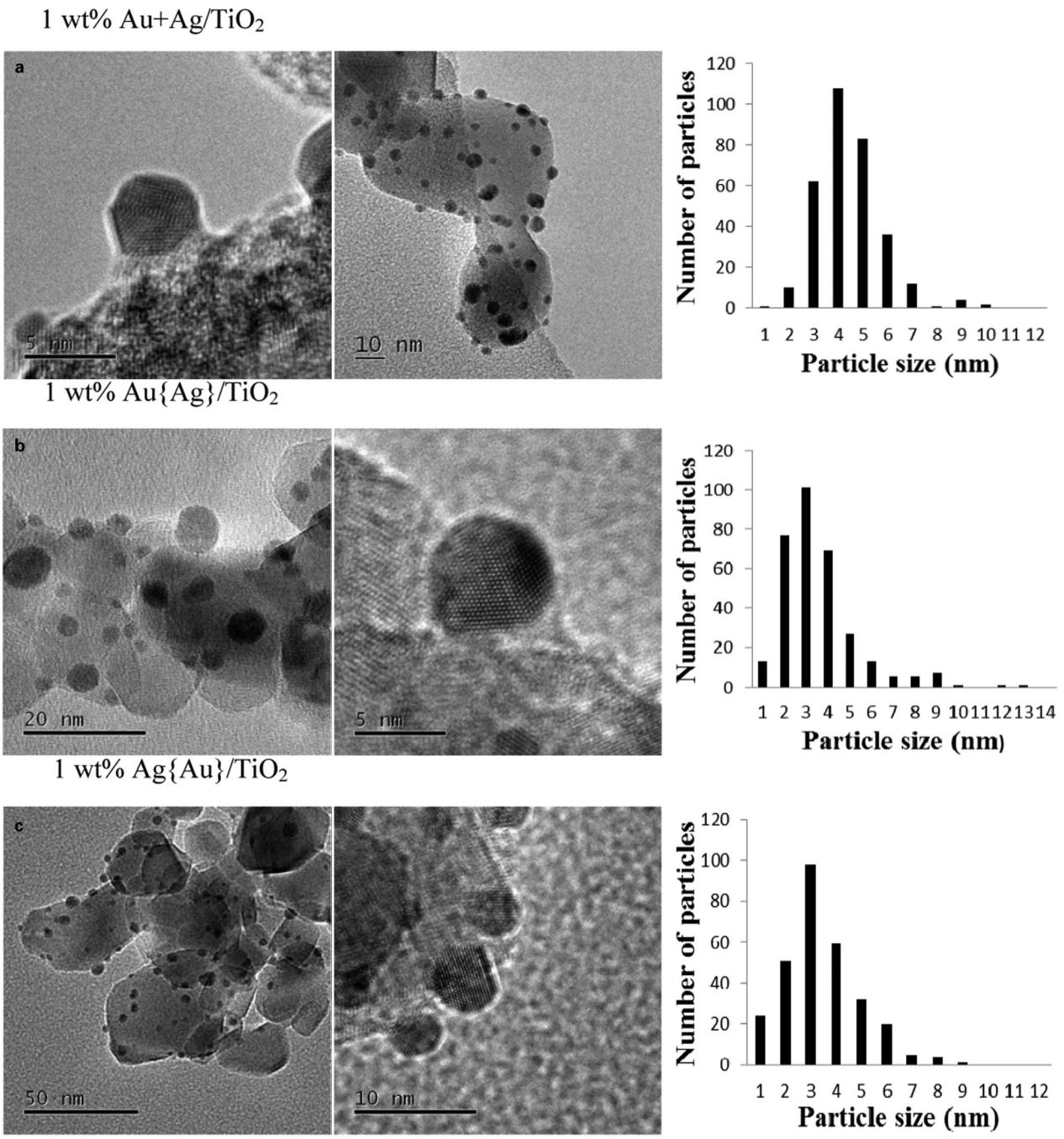

Figure 3 Representative bright field TEM micrographs (low and high resolution) and corresponding particle size distributions for *a* 1 wt-%Au + Ag/TiO_2, *b* 1 wt-%Au{Ag}/TiO_2 and *c* 1 wt-%Ag{Au}/TiO_2 catalysts. Samples were dried overnight at 120°C

energies also depend on the surrounding fluid and the adsorbed stabilizers.

Catalytic testing

Effect of gold loading and heat treatment on photocatalytic performance

Figures S5 and S6 in the Supplementary Material show the H_2 evolution as a function of time for the dried and calcined Au/TiO_2 catalysts respectively. The majority of the dried and calcined Au/TiO_2 catalysts showed an almost linear H_2 concentration dependence as a function of reaction time. Figure 6 presents H_2 evolution rates from methanol over Au/TiO_2 catalysts (dried and calcined at 400°C) as a function of Au loading. It is evident that the catalytic performance of the calcined catalysts was improved by a factor of 2–3 with respect to the dried-only catalysts. Taking into account that there is also an increase of the mean particle size between the dried and calcined Au/TiO_2 catalysts (i.e. from ~3 to ~5 nm), the main reason for the enhancement of the catalytic activity of the latter may be related to the removal of the PVA ligands around the metal particle and as well as from the TiO_2 surface. It is known from TGA studies the effective removal of PVA from the Au/TiO_2 catalyst requires heating above 250°C.[35]

We observed a low rate for hydrogen production for low (0.1 wt-%Au) and high (5 wt-%Au) metal loadings, whereas with intermediate metal loading levels between 0.2 and

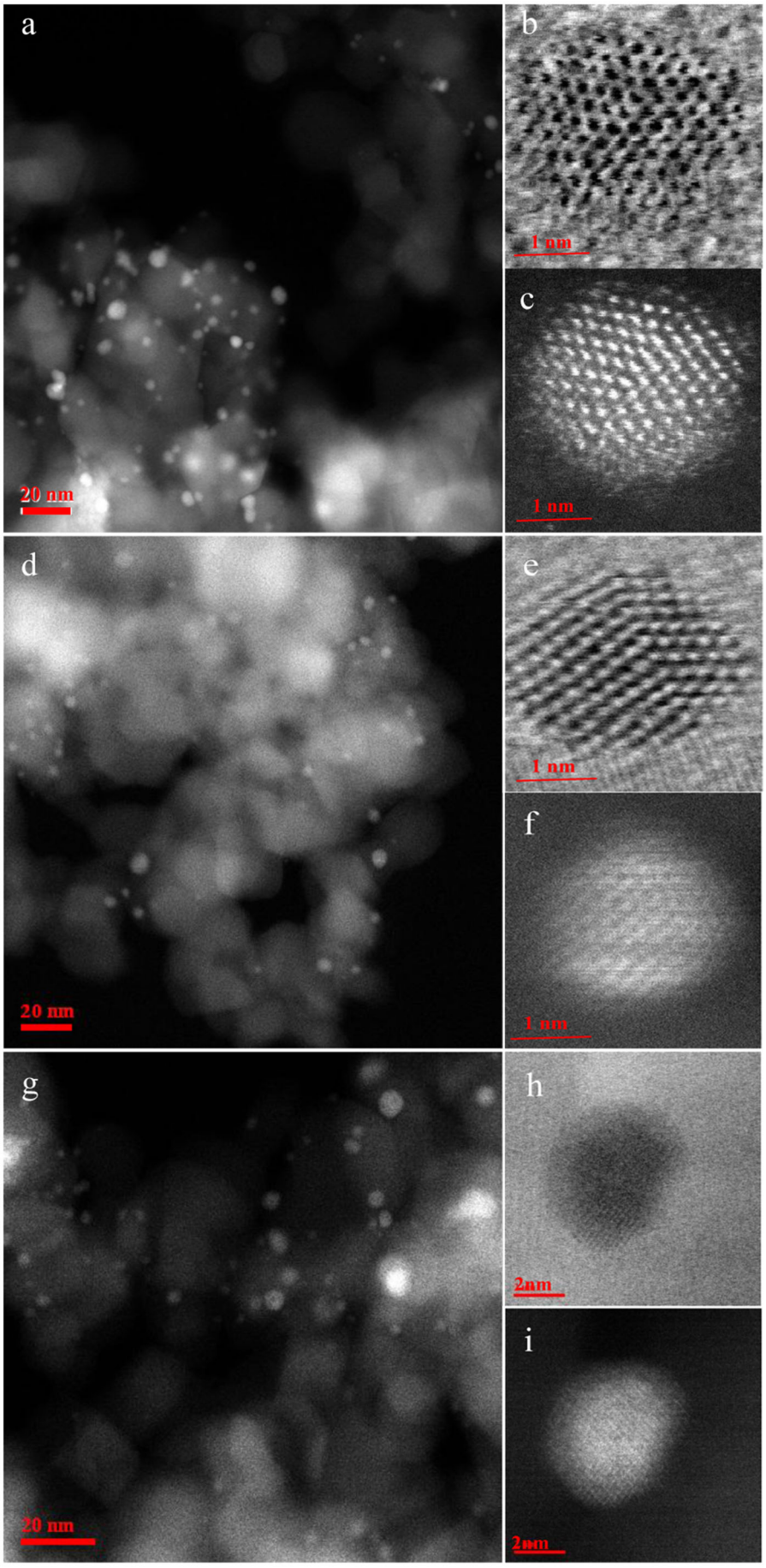

Figure 4 Representative low magnification HAADF images and high magnification BF– and HAADF–STEM images of *a,b,c* 1 wt-%(Au + Ag)/TiO_2; *d,e,f* 1 wt-%Au{Ag}/TiO_2; *g,h,i* 1 wt-%Ag{Au}/TiO_2 catalysts

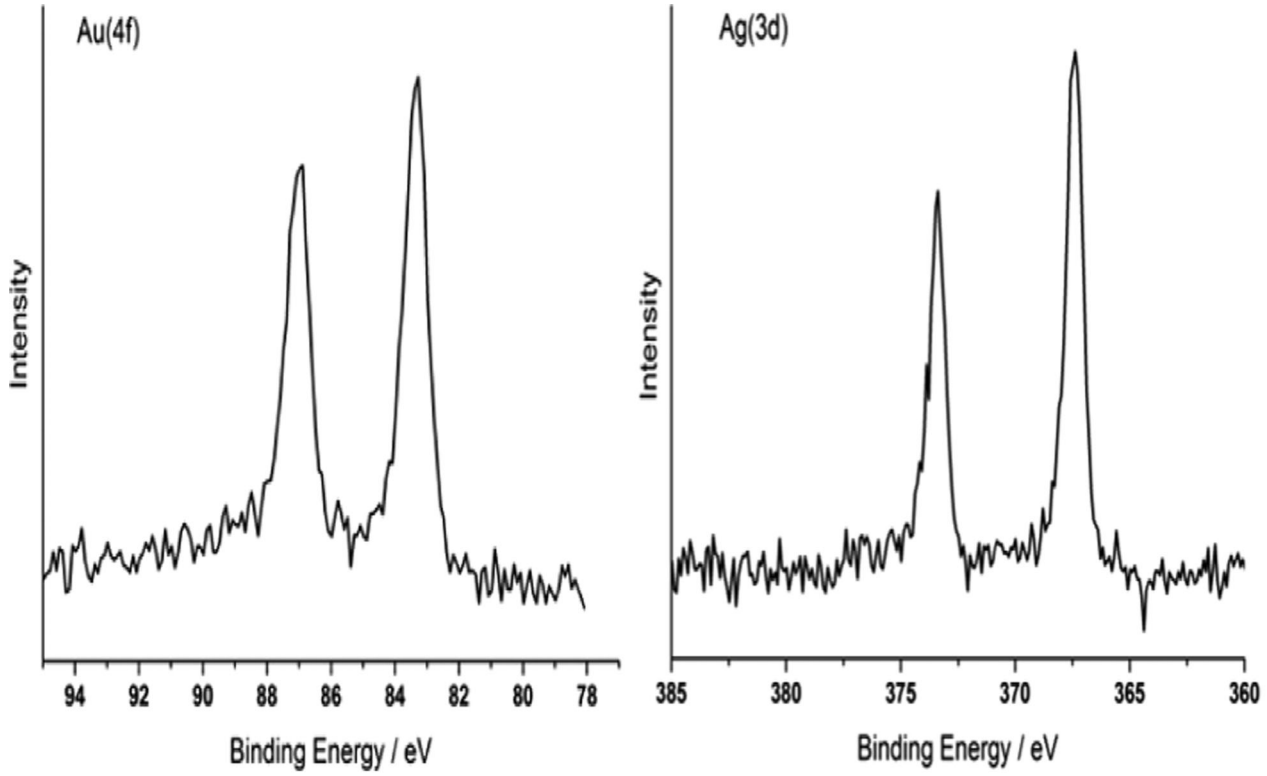

Figure 5 Spectra (XPS) of *a* Au(4f) and *b* Ag(3d) region of Ag{Au}/TiO_2 catalyst

2 wt-%Au, the highest H_2 production rates were observed. In fact, we observed two maximum rates at loadings of 0.4 and 1 wt-%Au for the dried catalysts, whereas for the calcined Au supported catalysts the maximum rates were found for loadings of 0.4 and 2 wt-%, which is in agreement with previous published results for catalysts made by the incipient wetness technique.[36] The decrease in H_2 evolution rate above 2 wt-% can be attributed to a reduction of the available metal support sites since both metal and support sites are essential for the reaction. On the other hand, it is expected that Au atoms at the interface with TiO_2 will eventually enhance the amount of trapped electrons that will be available for the reduction of hydrogen ions to hydrogen molecules. An important question to consider is the cause of the dual peak for the hydrogen production rate. Previous studies have shown that different morphologies and structures of gold can exist, depending on the gold loading and calcination temperature[37–40] and therefore could affect catalytic activity. We have previously shown that in the case of Au/TiO_2 catalysts synthesized by sol immobilization method a mixture of cub-octahedral, singly twinned and multiply twinned morphologies (icosahedral and decahedral particles) are present.[35] Moreover, a heat treatment has a substantial effect on the morphology of the Au particles supported onto TiO_2 where an increase in heat treatment temperature from 120 to 400°C leads to an increase in the formation of gold particles with cub-octahedral morphology and the Au particles form an extended flat interface structure with the crystalline TiO_2 substrate. Therefore, the combination of these parameters can explain partly the observation of two peaks in H_2 production rate in the case of Au/TiO_2 catalysts as a function of Au loading.

Table 3 Binding energies and Au/Ag atomic ratios of various supported Au, Ag, Au–Ag (1/1 atomic ratio) catalysts as determined by XPS investigated in our photocatalytic experiments

Catalyst	BE/eV $Au4f_{7/2}$	BE/eV $Ag3d_{5/2}$	Au/Ag atomic ratio
Au/TiO_2	83.4	…	…
Ag/TiO_2	…	368.1	…
Au+Ag/TiO_2	83.4	367.5	2.00
Ag{Au}/TiO_2	83.3	367.3	1.14
Au{Ag}/TiO_2	83.6	367.6	1.24

Photocatalytic activity of Au–Ag catalysts

Figure S7 in the Supplementary Material shows H_2 evolution of Au–Ag/TiO_2 catalysts as a function of reaction time. Similar to the case of the Au/TiO_2 catalysts, a linear H_2

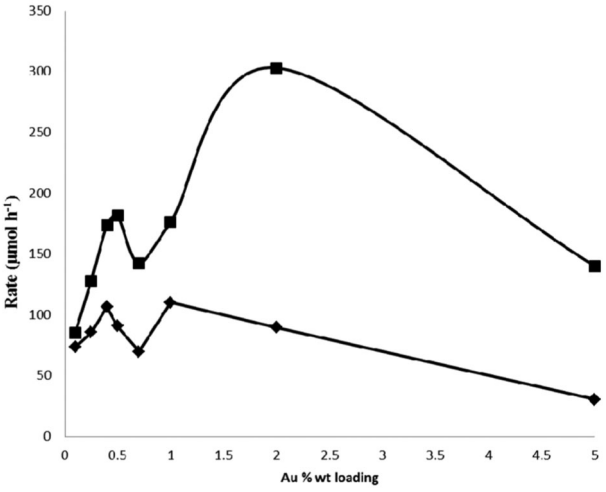

Figure 6 Rate of hydrogen production versus gold weight loading of dried (♦) and calcined (■) Au/TiO_2 catalysts

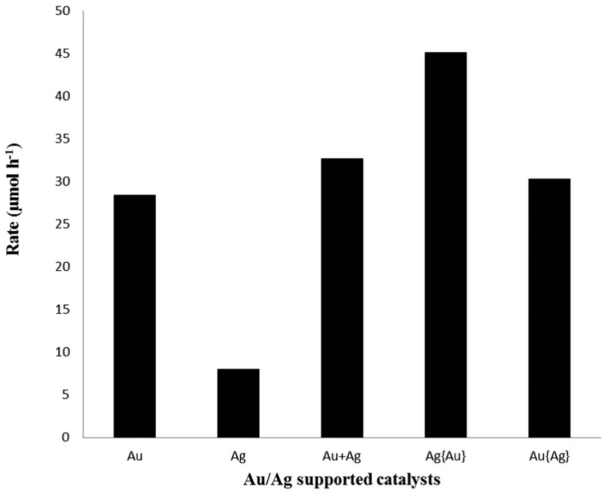

Figure 7 Rate of hydrogen production from various Au, Ag, Au–Ag nanoparticles supported on TiO_2 and dried at 120°C

concentration dependence was observed with reaction time. Figure 7 shows the rate of H_2 production averaged over 3 h of reaction and it is evident that the Ag{Au}/TiO_2 catalysts in particular showed a higher H_2 evolution rate than the monometallic Au and Ag catalysts. The order of activity for the Au–Ag supported catalysts was Ag{Au}/TiO_2>Au{Ag}/TiO_2 ~ Au + Ag/TiO_2 ~ Au/TiO_2>Ag/TiO_2. These results reveal that the most effective method for the synthesis of active Au–Ag catalysts for this reaction is when sequential Ag sol formation was carried out on a pre-formed Au sol [Ag{Au}], suggesting that the order of addition and reduction of metal has a significant effect on activity. Taking into account that the mean particle size is similar for the whole series of Au–Ag/TiO_2 catalysts (around 4 nm), the difference in terms of catalytic activity displayed may be attributed to several parameters, such as the formation of alloyed or core–shell structures and the relative electron affinities of Au and Ag. Since Au has a higher electron affinity than Ag (2.3 versus 1.3), it is therefore reasonable to expect that its electron trapping capability will be enhanced relative to Ag. In the case of the three different Au–Ag catalyst variants we have used methodologies based on co-reduction and consecutive addition/reduction of metal where we expect that the development of Au–Ag alloyed and core–shell structures will be developed respectively. Taking into account the electron affinity values and XPS data, we observed a similar or a slight lower BE of Au(4f) in the series of Au–Ag/TiO_2 catalysts with respect to monometallic Au/TiO_2 catalysts, which may reflect some charge transfer from Ag to Au atoms. A slightly lower BE for Au was observed with respect to Au/TiO_2 (BE of Au4$f_{7/2}$ at 83.4 eV) in the case of Ag{Au}/TiO_2, while for the Au{Ag}/TiO_2 material it was higher, implying that the electronic transfer between Ag and Au atoms was only affected in a minor way by the preparation methodology used. Considering the fact that a major role of supported metal nanoparticles in the context of photocatalytic reactions is to increase the lifetime of photo excited electrons, then this may be the underlying cause of enhancement of catalytic activity. In turn this enhancement of electron transfer from Ag to Au atoms could make them a reservoir for the capture of photo excited electrons and lead to higher catalytic activity. On the contrary, when the BE of Au is higher or for Au + Ag/TiO_2 and Ag{Au}/TiO_2 catalysts than the BE of Au for the Au/TiO_2 catalyst we expect a lower degree of electron transfer between Ag and Au atoms and therefore a lower capability of the Au–Ag metallic nanoparticles to act as an electron reservoir. In addition to these effects we must also note that the effective surface area of the Ag in the Ag{Au} sample is much higher than it is in the monometallic Ag, due to the much lower average particle size, which may further enhance activity, at least in comparison with the monometallic Ag/TiO_2 catalyst.

Conclusions

The photocatalytic production of H_2 was studied over Au/TiO_2, Ag/TiO_2 and Au–Ag/TiO_2 catalysts synthesized by the sol–immobilization method. The effect of gold loading and heat treatment over Au/TiO_2 catalysts showed that the maximum rate of H_2 production was observed for Au loadings of 1–2 wt-%. The heat treatment in air at 400°C was essential for improving the rates of H_2 production by a factor of 2–2.5 for the monometallic Au/TiO_2 sol–immobilized catalysts, probably due to the removal of PVA molecules. For the bimetallic Au–Ag/TiO_2 catalysts by using methods A (simultaneous reduction of the two metals) and C (reduction of Ag precursor followed by addition and reduction of the Au precursor) we observed some enhancement of photocatalytic activity with respect to monometallic Au/TiO_2 catalyst and a significant increase with respect to monometallic Ag/TiO_2 catalyst. However, when preparing bimetallic Au–Ag/TiO_2 catalysts using method B (reduction of Au precursor followed by addition and reduction of the second Ag precursor) we observed a significant increase in photocatalytic activity by factors ranging between 1.6 and 7 times with respect to the corresponding Au/TiO_2 and Ag/TiO_2 monometallic catalysts. These results show that the order of the metal addition and reduction is significant for the preparation of active Au–Ag/TiO_2 photocatalysts and in improving the activity of Ag based catalysts.

Conflicts of interest

The authors declare no conflicts of interest.

Acknowledgements

We are grateful to the Cardiff Catalysis Institute and to Research Complex at Harwell for the provision of several of the facilities used in this work, and to the EPSRC for studentship funding to JK and WJ.

References

1. M. Bowker: *Green Chem.*, 2011, **13**, 2235–2246.
2. A. Fujishima and K. Honda: *Nature*, 1972, **238**, 37–38.
3. A. L. Linsebigler, G. Q. Lu and J. T. Yates: *Chem. Rev.*, 1995, **95**, 735–758.
4. H. Park, W. Choi and M. R. Hoffmann: *J. Mater. Chem.*, 2008, **18**, 2379–2385.
5. M. Murdoch, G. I. N. Waterhouse, M. A. Nadeem, J. B. Metson, M. A. Keane, R. F. Howe, J. Llorca and H. Idriss: *Nat. Chem.*, 2011, **3**, 489–492.
6. P. Shen, S. Zhao, D. Su, Y. Li and A. Orlov: *Appl. Catal. B: Environ.*, 2012, **126B**, 153–160.
7. A. S. K. Hashmi and G. J. Hutchings: *Angew. Chem. Int. Ed.*, 2006, **45**, 7896–7936.

Maney Publishing

8. C. Della Pina, E. Falletta, L. Prati and M. Rossi: *Chem. Soc. Rev.*, 2008, **37**, 2077–2095.
9. T. Mallat and A. Baiker: *Chem. Rev.*, 2004, **104**, 3037–3058.
10. A. Abad, P. Concepción, A. Corma and H. Garcia: *Angew. Chem. Int. Ed.*, 2005, **44**, 4066–4069.
11. P. Vinod, K. Wilson and A. F. Lee: *J. Chem. Technol. Biotechnol.*, 2011, **86**, 161–171.
12. D. Mott, N. T. B. Thuy, Y. Aoki and S. Maenosono: *Philos. Trans. R. Soc. A*, 2010, **368A**, 4275–4292.
13. M. S. Shore, J. Wang, A. C. Johnston-Peck, A. L. Oldenburg and J. B. Tracy: *Small*, 2011, **7**, 230–234.
14. S. Nishimura, A. T. N. Dao, D. Mott, K. Ebitani and S. Maenosono: *J. Phys. Chem. C*, 2012, **116C**, 4511–4516.
15. S. Sarina, E. R. Waclawik and H. Zhu: *Green Chem.*, 2013, **15**, 1814–1833.
16. C. Han, X. Yang, G. Gao, J. Wang, H. Lu, J. Liu, M. Tong and X. Liang: *Green Chem.*, 2014, **15**, 3603–3615.
17. S. Oros-Ruiz, R. Zanella, S. E. Collins, A. Hernández-Gordillo and R. Gómez: *Catal. Commun.*, 2014, **47**, 1–6.
18. A. Dickinson, D. James, N. Perkins, T. Cassidy and M. Bowker: *J. Mol. Catal. A*, 1999, **146A**, 211–221.
19. M. Bowker, D. James, P. Stone, R. Bennett, N. Perkins, L. Millard, J. Greaves and A. Dickinson: *J. Catal.*, 2003, **217**, 427–433.
20. H. Bahruji, M. Bowker, P. R. Davies, L. Saeed Al-Mazroai, A. Dickinson, J. Greaves, D. James, L. Millard and F. Pedrono: *J. Photochem. Photobiol.*, 2010, **216**, 115–118.
21. H. Bahruji, M. Bowker, P. R. Bowker and F. Pedrono: *Appl. Catal. B: Environ.*, 2011, **107B**, 205–209.
22. L. Prati and G. Marta: *Gold Bull.*, 1999, **32**, 96–101.
23. N. Dimitratos, A. Villa, D. Wang, F. Porta, D. Su and L. Prati: *J. Catal.*, 2006, **244**, 113–121.
24. A. Villa, D. Wang, N. Dimitratos, D. Su, V. Trevisan and L. Prati: *Catal. Today*, 2010, **150**, 8–15.
25. M. Comotti, W. C. Li, B. Spliethoff and F. Schüth: *J. Am. Chem. Soc.*, 2006, **128**, 917–924.
26. A. Villa, N. Janjic, P. Spontoni, D. Wang, D. S. Su and L. Prati: *Appl. Catal. A*, 2009, **364A**, 221–228.
27. R. C. Tiruvalam, J. Pritchard, N. Dimitratos, J. A. Lopez-Sanchez, J. K. Edwards, A. F. Carley, G. J. Hutchings and C. J. Kiely: *Faraday Discuss.*, 2011, **152**, 63–86.
28. N. Dimitratos, J. A. Lopez-Sanchez, D. Morgan, A. Carley, L. Prati and G. J. Hutchings: *Catal. Today*, 2007, **122**, 317–324.
29. W. Wang, S. Efrima and O. Regev: *Langmuir*, 1998, **14**, 602–610.
30. S. Link, Z. L. Wang and M. A. El-Sayed: *J. Phys. Chem. B*, 1999, **103B**, 3529–3533.
31. G. Compagnini, E. Messina, O. Puglisi, R. S. Cataliotti and V. Nicolosi: *Chem. Phys. Lett.*, 2008, **457**, 386–390.
32. X. Liu, X. Yang, T. Zhang, C. Y. Mou, D. S. Su and J. Li: *Chem. Mater.*, 2008, **21**, 410–418.
33. M. P. Mallin and C. J. Murphy: *Nano Letters*, 2002, **2**, 1235–1237.
34. H. L. Jiang, T. Akinta, T. Ishida, M. Haruta and Q. Xu: *J. Am. Chem. Soc.*, 2011, **133**, 1304–1306.
35. J. A. Lopez-Sanchez, N. Dimitratos, C. Hammond, G. J. Brett, L. Kesavan, S. White, P. Miedziak, R. Tiruvalam, R. L. Jenkins, A. F. Carley, D. Knight, C. J. Kiely and G. J. Hutchings: *Nat. Chem.*, 2011, **3**, 551–556.
36. M. Bowker, L. Millard, J. Greaves, J. James and J. Soares: *Gold Bull.*, 2004, **37**, 170–173.
37. P. Claus, A. Brückner, C. Mohr and H. Hofmeister: *J. Am. Chem. Soc.*, 2000, **122**, 11430–11439.
38. M. S. Chen and D. W. Goodman: *Science*, 2004, **306**, 252–255.
39. A. A. Herzing, C. J. Kiely, A. F. Carley, P. Landon and G. J. Hutchings: *Science*, 2008, **321**, 1331–1335.
40. N. Dimitratos, J. A. Lopez-Sanchez, D. Morgan, A. F. Carley, R. Tiruvalam, C. J. Kiely, D. Bethell and G. J. Hutchings: *Phys. Chem. Chem. Phys.*, 2009, **11**, 5142–5153.